

Color- flavor dependence of the Nambu-Jona-Lasinio model and QCD phase diagram

Aftab Ahmad and Ali Murad

Institute of Physics, Gomal University, 29220, D.I. Khan, Khyber Pakhtunkhaw, Pakistan.

E-mail: aftabahmad@gu.edu.pk, alimuradeng@gmail.com

Abstract. We study the dynamical chiral symmetry breaking/restoration for the various numbers of light quarks flavors N_f and colors N_c , using the Nambu-Jona-Lasinio (NJL) model of quarks, dressed with a color-flavor dependence of effective coupling. Initially, we set $N_f = 2$, and varying the number of colors N_c , we find that the dynamical chiral symmetry is broken when N_c exceeds to its critical value $N_c^c \approx 2.2$. Secondly, we take $N_c = 3$, and varying N_f , we observed that the dynamical chiral symmetry is restored when N_f reaches to its critical value $N_f^c \approx 8$. The strong interplay observed between N_c and N_f , i.e., N_c anti-screens the strong interactions by strengthening the dynamical mass and quark-antiquark condensate, while N_f screens the strong interaction by suppressing both the parameters. We further sketch the quantum chromodynamics (QCD) phase diagram at finite temperature T and quark chemical potential μ for various N_c and N_f . At finite T and μ , we observed that the critical number of colors N_c^c enhances while the critical number of flavors N_f^c suppresses as T and μ increases. Of course, the parameters T and μ produces the screening effect. Consequently, the critical temperature T_c , μ_c and co-ordinates of the critical endpoint (T_c^E, μ_c^E) in the QCD phase diagram enhances as N_c increases while suppresses when N_f increases. Our findings agree with the Lattice QCD and Schwinger-Dyson equations predictions.

Keywords: Chiral symmetry breaking, Schwinger-Dyson equation, Finite temperature and density, QCD phase diagram

1. Introduction

Quantum Chromodynamics (QCD) is a well-established theory of strong color interaction among the quarks and gluons. Two major aspects of the QCD are the asymptotic freedom (ultraviolet regime) [1, 2] and quark confinement (infrared regime) [3]. In the asymptotic freedom, the quarks interact weakly at a short distance inside the hadrons. On the other hand, at a large distance (or at low energy) the quarks are confined and never exist in isolation. Besides the color confinement, the dynamical chiral symmetry breaking is another important property of the low-energy QCD, which is related to the dynamical mass generation of the quarks. It is well known that in the fundamental representation of the gauge group $SU(N_c)$, the QCD exhibits confinement and dynamical chiral symmetry breaking with the small number of light quark flavors N_f . But for larger N_f , it is believed that there is a critical value N_f^c above which, the chiral symmetry restores, and quarks become unconfined [4, 5, 6]. This value N_f^c , must be smaller than the upper limit of the critical value where asymptotic freedom is appeared to exist is $N_f^{A,c} = (11/2)N_c$ [2], for $N_c = 3$ with a gauge group $SU(3)$, this critical number is $N_f^{A,c} = 16.5$. Hence, the QCD theory is said to be conformal in the infrared, guided by an infrared fixed point (i.e., a point at which the β -functions for the QCD couplings vanishes), see for example in detail [7, 8, 9, 10, 11, 12]. The region $N_f^c \lesssim N_f < N_f^{A,c}$, is often called as the “conformal zone” [4, 13]. At or near the upper end ($N_f \lesssim N_f^{A,c}$) of the conformal zone, the infrared fixed point lies in the weakly interacting region and can be dealt with perturbative techniques of QCD. On the other hand, around the lower end ($N_f \sim N_f^c$), the infrared fixed point shift toward the strongly interacting region where the coupling is sufficiently strong as N_f decreases and thus, the system enters a phase where the chiral symmetry breaks and quarks become confined. In this situation, the perturbative approaches to QCD are inconceivable and thus, the non-perturbative techniques are useful tool. Lattice QCD simulations [6, 14, 15, 16, 17], as well as the continuum methods of QCD [5, 18, 19, 20, 21, 22], in the fundamental $SU(3)$ representation, emphasized that the chiral symmetry restoration and deconfinement phases exiting when N_f reaches to the conformal zone $8 \lesssim N_f^c < 12$. QCD theory with a larger number of colors N_c , in the fundamental $SU(N_c)$, representation, also plays a significant role in the infrared domain. It has been discussed in [22], that the dynamical chiral symmetry also breaks when N_c exceeded to a critical value $N_c^c \approx 2.2$. The increasing number of colors N_c , anti-screens the strong interactions and enhances the dynamical mass generation near and above N_c^c . The large N_c , also effects the critical value of flavors N_f^c , that is, N_f^c shifts toward its higher values as N_c increases. The N_c and N_f compete each other, i.e., N_f screens the strong interactions in contrast to the N_c anti-screening effect [22].

Besides the N_c and N_f , the infrared domain of QCD is also affected by the presence of heat bath T . It is believed that at zero or low T , the fundamental degrees of freedom of low energy QCD are the color-singlet (confined) hadrons, whereas, at high T , when T reaches to its critical value T_c , the interaction becomes weak and thus, causing hadrons

to melt down into a new phase, where now the quarks and gluons becomes the new degrees of freedom. The chiral symmetry is restored and deconfinement of quarks occurs in this new phase. Lattice QCD calculation [23, 24, 25, 26, 27, 28, 29], Schwinger-Dyson equation [30, 31, 32, 33, 34, 35, 36, 37, 38, 39] and another effective model of QCD [40, 41, 42, 43, 44, 45, 46] claims that the nature of this transition is cross-over in the presence of finite current quark mass m . Similarly, upon increasing quark chemical potential μ , the same physical picture prevails, but the nature of the phase transition changes from cross-over to the first-order at some point, known as the critical endpoint in the QCD phase diagram, usually drawn in the $T - \mu$ plane. Experimentally, there is a strong motivation regarding the study of phase transition in the Heavy-Ion Collision at the Large Hadron Collider (LHC) in CERN, the Relativistic Heavy Ion Collider (RHIC) at Brook Heaven National Laboratory (BNL), and Compact Baryonic Matter (CBM) experiments. The study of low energy QCD for higher quark flavors N_f and N_c also plays a significant role in physics beyond the standard model (BSM), and its extension to the QCD phase diagram at finite T and μ , where different phases of QCD exists, i.e., quark-gluon plasma, quarkonia matter, neutron star environment and the color-favor-locked region of the QCD phase diagram.

Our aim and motivation of this work is to investigate the critical number of colors N_c and flavors N_f for the chiral symmetry breaking and restoration at zero T , finite T and μ . Furthermore, we are interested to draw QCD phase diagram in the $T - \mu$ plane for various N_c and N_f . We use the effective Nambu-Jona-Lasinio (NJL) model [47], in the Hartree-Fock mean-field approximation, dressed with the number of quark flavors N_f and colors N_c . NJL model has several features and is commonly used in the literature. The Dynamical chiral symmetry breaking and its restoration are some of the main features of this model. However, it does not support the phenomenon of quark confinement.

This article is organized as follows: In Sec. 2, we introduce the general formalism of the NJL model at $T = 0$, at finite T and μ . We discuss the numerical solution of the gap equation to study the dynamical chiral symmetry breaking and its restoration for higher colors N_c and flavors N_f in Sec. 3. We present the numerical solution of the gap equation for higher N_c and N_f and at finite temperature T in Sec. 4. In Sec. 5, we display the numerical solution of the gap equation at finite chemical potential μ , for various N_c and N_f . We sketch the phase diagram in the $T - \mu$ plane for various N_c and N_f in the Sec. 6. In the last Sec. 7, we demonstrate the summary and conclusions of this work.

2. General Formalism of the NJL Model

We start QCD in an effective manner through NJL Lagrangian [47]:

$$\mathcal{L} = \bar{q}(i \not{\partial} - m)q + \frac{G}{2}[(\bar{q}q)^2 + (\bar{q}i\gamma_5\vec{\tau}q)^2], \quad (1)$$

where the four-Fermi interactions term contains a scalar and an axial-vector interaction piece (τ representing the Pauli matrices in isospin space) and G is the coupling of the

theory. Such a Lagrangian Eq. (1) describes the dynamical chiral symmetry breaking, which can be triggered through Schwinger-Dyson equations (SDE) for the dressed quark propagator, can be written as

$$S^{-1}(p) = S_0^{-1}(p) + \Sigma(p). \quad (2)$$

Here S^{-1} is the inverse of the dressed quark propagator:

$$S^{-1}(p) = i\gamma \cdot p + M, \quad (3)$$

with M is the dynamical quark mass, γ^μ are the Dirac 4×4 gamma matrices and p^μ are the four-momenta. The inverse of the free quark propagator S_0^{-1} is defined as

$$S_0^{-1}(p) = i\gamma \cdot p + m, \quad (4)$$

where m is the bare quark mass, which we may set equal to zero in the chiral limit. The $\Sigma(p)$ is the quark self energy which can be written as

$$\Sigma(p) = \int \frac{d^4k}{(2\pi)^4} g^2 \Delta_{\mu\nu}(p-k) \frac{\lambda^a}{2} \gamma_\mu S_f(k) \frac{\lambda^a}{2} \Gamma_\nu(p,k), \quad (5)$$

here g is the QCD coupling constant, Γ_ν is the dressed quark-gluon vertex, $\Delta_{\mu\nu}$ is the gluon propagator and $S(k)$ is the dressed quark propagator:

$$S(k) = \frac{i\gamma \cdot p + MI}{p^2 - M^2 + i\epsilon}, \quad (6)$$

here $i\epsilon$ is the causality factor, introduced to exclude the singularity from the propagator, the λ^a are the usual Gell-Mann's matrices. In the $SU(N_c)$ representation the Gell-Mann's matrices satisfies the following identity:

$$\sum_{a=1}^8 \frac{\lambda^a}{2} \frac{\lambda^a}{2} = \frac{1}{2} \left(N_c - \frac{1}{N_c} \right). \quad (7)$$

In NJL model, we set

$$g^2 \Delta_{\mu\nu} = G \delta_{\mu\nu}, \quad (8)$$

where G is the effective coupling. The effective coupling G must exceeds a critical value G_c , in order to describes the dynamical chiral symmetry breaking. When G is greater than its critical value G_c , a nontrivial solution to the QCD gap equation bifurcates from the trivial one, see for example Ref. [48]. Substituting Eqs. (3),(4),(5),(6),(7),(8), in Eq. (2) and taking the trace over the Dirac, colors and flavors components, the quark gap equation is given as

$$M = m + 8i\mathcal{G}^{N_c}(N_f) \int \frac{d^4k}{(2\pi)^4} \frac{M}{k^2 - M^2 + i\epsilon}, \quad (9)$$

where M is the dynamical mass and $\mathcal{G}^{N_c}(N_f)$ is the effective coupling in which the color and flavor factors are incorporated as

$$\mathcal{G}^{N_c}(N_f) = \left[\frac{1}{2} \left(N_c - \frac{1}{N_c} \right) \right] G(N_f). \quad (10)$$

To study the gap equation for the various number of flavors, we needs to modify the flavor sector $G(N_f)$ of the effective coupling $\mathcal{G}^{N_c}(N_f)$, in such a way that it must give solutions

of the gap equation for the higher number of flavors. We shall use this modification as our modeling and it will help us to find out the critical number of flavors N_f^c or colors N_c^c for the chiral symmetry breaking or restoration. We adopted a similar way of modeling used by [5, 22], where the critical number of flavors N_f^c obtained from Schwinger-Dyson equations. According to Ref. [5, 22], the dynamically generated mass M should have the following kind of relationship with the critical number of flavors N_f^c :

$$M \sim \sqrt{1 - \frac{N_f}{N_f^c}}, \quad (11)$$

where N_f^c denote the critical number of flavors. To find the critical number of flavors N_f^c , we modified the factor $G(N_f)$ of Eq. (10) in similar fashion as [22]:

$$G(N_f) \longrightarrow \frac{9}{2}G\sqrt{1 - \frac{(N_f - 2)}{\mathcal{N}_f^c}}, \quad (12)$$

with $\mathcal{N}_f^c = N_f^c + \eta$, is some guess values of critical number of flavors. Our modification of the effective coupling is almost the same as in Ref. [22], but slightly different by a factor of 9/2, this is because, the effective coupling model of Ref. [22], uses a symmetry preserving, local four-point contact interaction model of quarks with the quantum numbers of a massive-gluon exchange and in the scalar-pseudoscalar channel this is Fierz equivalent to the NJL-Lagrangian Eq. (1) [43].

To obtain the N_f^c , we set $\eta = 2.3$, which lies in the range as predicted in [22] by considering $N_f^c = 8$. It has been demonstrated in the Ref. [22] that the appearance of the parameter η is because of the factor $(N_f - 2)$ in Eq. (12). For fixed $N_c = 3$ and $N_f = 2$, our modified NJL effective coupling $\mathcal{G}^{N_c}(N_f) \rightarrow GN_fN_c$, normally used in NJL model gap equation [41].

The four-momentum integral in Eq. (9), can be solved by splitting the four-momentum into time and space components. We denote the space part by a bold face latter \mathbf{k} and the time part by k_0 . Thus, the Eq. (9), can be written as

$$M = m + 8i\mathcal{G}^{N_c}(N_f)M \int_0^\infty \frac{d^3\mathbf{k}}{(2\pi)^4} \int_{-\infty}^{+\infty} \frac{dk_0}{k_0^2 - E_k^2 + i\epsilon}. \quad (13)$$

Here, $E_k = \sqrt{|\mathbf{k}|^2 + M^2}$, in which E_k denotes the energy per particle and \mathbf{k} is the 3-momentum. On integrating over the time component of Eq. (13), we can get the following expression:

$$M = m + 8i\mathcal{G}^{N_c}(N_f)M \int_0^\infty \frac{d^3\mathbf{k}}{(2\pi)^4} \frac{\pi}{iE_k} \quad (14)$$

In spherical polar coordinates $d^3\mathbf{k} = \mathbf{k}^2 d\mathbf{k} \sin\theta d\theta d\phi$ and performing the angular integration, we have from Eq. (14):

$$M = m + \frac{2\mathcal{G}^{N_c}(N_f)M}{\pi^2} \int_0^\infty d\mathbf{k} \frac{\mathbf{k}^2}{E_k}. \quad (15)$$

The integral occurring in Eq. (12) is a diverging integral and we also know that the NJL model is not renormalizable due to fermionic contact interaction. One can find different

kinds of regularization schemes used in the literature [40]. The regularization procedure we adopted in the present scenario is the three-dimensional (3d) momentum cut-off, where we remove the divergence by applying a certain high ultraviolet 3d-momentum cut-off Λ . So, Eq. (15) can be written as

$$M = m + \frac{2\mathcal{G}^{N_c(N_f)}M}{\pi^2} \int_0^\Lambda d\mathbf{k} \frac{\mathbf{k}^2}{E_k}. \quad (16)$$

On integrating Eq. (16), we have

$$M = m + \frac{\mathcal{G}^{N_c(N_f)}M}{\pi^2} \left[\Lambda\sqrt{\Lambda^2 + M^2} - M^2 \operatorname{arcsinh}\left(\frac{\Lambda}{M}\right) \right]. \quad (17)$$

In the present situation, the quark-antiquark condensate which serve as an order parameter for the chiral symmetry breaking is defined as

$$-\langle \bar{q}q \rangle = \frac{M - m}{2\mathcal{G}^{N_c(N_f)}}. \quad (18)$$

The finite temperature T and quark chemical potential μ version of the NJL-model gap equation Eq. (9), can be obtained by adopting the standard convention for momentum integration i.e.,

$$\int \frac{d^4k}{i(2\pi)^4} f(k_0, \mathbf{k}) \rightarrow T \sum_n \int \frac{d^3k}{(2\pi)^3} f(i\omega_n + \mu, \mathbf{k}), \quad (19)$$

with $\omega_n = (2n + 1)\pi T$ are the fermionic Matsubara frequencies. After doing some algebra, the gap equation Eq. (9), at finite T and μ , can be written as

$$M = m + 4\mathcal{G}^{N_c(N_f)}M \int_0^\Lambda \frac{d^3\mathbf{k}}{(2\pi)^3} \frac{1}{E_k} (1 - n_F(T, \mu) - \bar{n}_F(T, \mu)), \quad (20)$$

which is similar to the Eq. (17) in vacuum, but modified by the thermo-chemical parts. Where $n_F(T, \mu)$ and $\bar{n}_F(T, \mu)$ represents the Fermi occupation numbers for the quarks and antiquark, respectively, and defined as

$$n_F(T, \mu) = \frac{1}{e^{(E_k - \mu)/T} + 1}, \quad \bar{n}_F(T, \mu) = \frac{1}{e^{(E_k + \mu)/T} + 1}. \quad (21)$$

On further simplifying, we have

$$M = m + \frac{\mathcal{G}^{N_c(N_f)}M}{\pi^2} \left[\Lambda\sqrt{\Lambda^2 + M^2} - M^2 \operatorname{arcsinh}\left(\frac{\Lambda}{M}\right) \right] - \frac{\mathcal{G}^{N_c(N_f)}M}{\pi^2} \int_0^\Lambda d\mathbf{k} \frac{\mathbf{k}^2}{E_k} [n_F(T, \mu) + \bar{n}_F(T, \mu)] \quad (22)$$

If we set $\mu = T = 0$ in Eq. (22), we get $n_F = \bar{n}_F = 0$ and thus, we can retain the gap equation in vacuum i.e., Eq. (17). In the next section, we present numerical solution of the NJL-model gap equation for higher number of colors and flavors .

3. Dynamical chiral symmetry breaking/restoration for N_c and N_f

In this section, we numerically solve the gap equation Eq. (17), with a particular choice of the parameters i.e., $\Lambda = 587.9$ MeV, $G = 2.44/\Lambda^2$ and $m = 5.6$ MeV, which were fitted to reproduce the pions mass in the NJL model, used in [41]. The solution of our gap equation with modified color-flavor dependence effective coupling Eq. (10), for two light flavors $N_f = 2$ (i.e., up and down), and for $N_c = 3$, yields the dynamical mass $M = 399$ MeV. We calculated the value corresponding quark-antiquark condensate from Eq. (18), which is in this case $-\langle\bar{q}q\rangle^{1/3} = 250$ MeV. In this scenario, our results are consistent with that obtained in [41], for $N_f = 2$ and $N_c = 3$. Next, we need to solve the gap equation Eq. (17), for various number of colors N_c and flavors N_f . Initially, we solve the gap equation for fixed flavors $N_f = 2$, but for the various number of colors N_c and plotted the dynamically generated mass in Fig. 1, as a function of N_c . We find that the dynamical chiral symmetry is partially broken when the number of colors N_c exceeds a critical value $N_c = N_c^c$ and remains broken for larger values of N_c . The corresponding quark-antiquark condensate $-\langle\bar{q}q\rangle^{1/3}$ is shown in the Fig. 2. The critical number of colors N_c^c is obtained from the inflection point of the color-gradient of the quark-antiquark condensate $-\partial_{N_c}\langle\bar{q}q\rangle^{1/3}$ and is depicted in the Fig. 3. It is clear from the Fig. 3 that the dynamical chiral symmetry is partially broken above $N_c^c \approx 2.2$, and thus, consistent with the predicted value, obtained in Ref. [22].

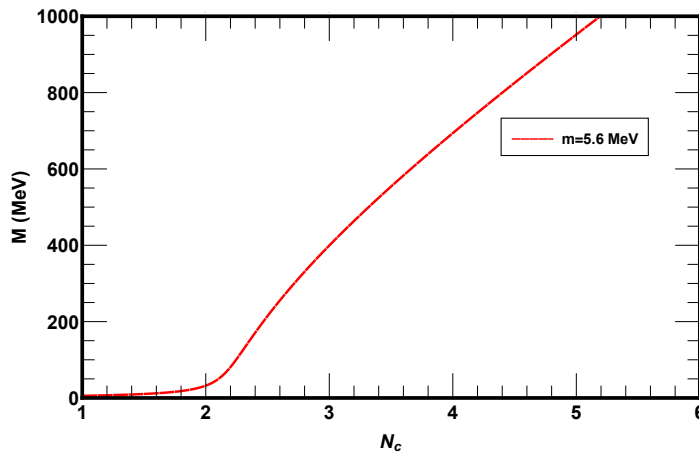


Figure 1. Behavior of the dynamical mass as a function of various number of colors N_c for two flavors $N_f = 2$.

Next, we consider $N_c = 3$ and solve the gap equation Eq. 17, for various number of flavors N_f , as shown in the Fig. 3. The plot demonstrates that the dynamically generated mass monotonically decreases with the increase of N_f until it reaches a critical value N_f^c , where the dynamical mass vanishes and only bare quark mass survives and thus, the chiral symmetry is partially restored above N_f^c . In Fig. 5, we plotted the quark-antiquark condensate $-\langle\bar{q}q\rangle^{1/3}$ as a function of N_f and its flavor-gradient $-\partial_{N_f}\langle\bar{q}q\rangle^{1/3}$ is depicted in the Fig. 6. Thus, we obtained the critical number of flavors $N_f^c \approx 8$ from the

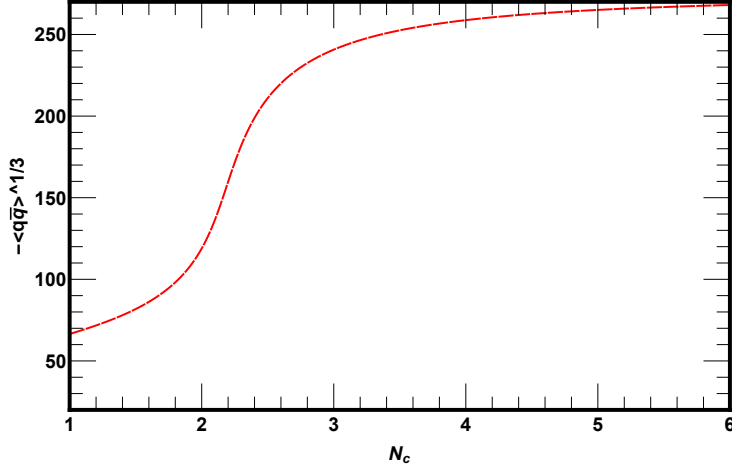


Figure 2. Quark-antiquark condensate plotted as a function of number of colors N_c for $N_f = 2$.

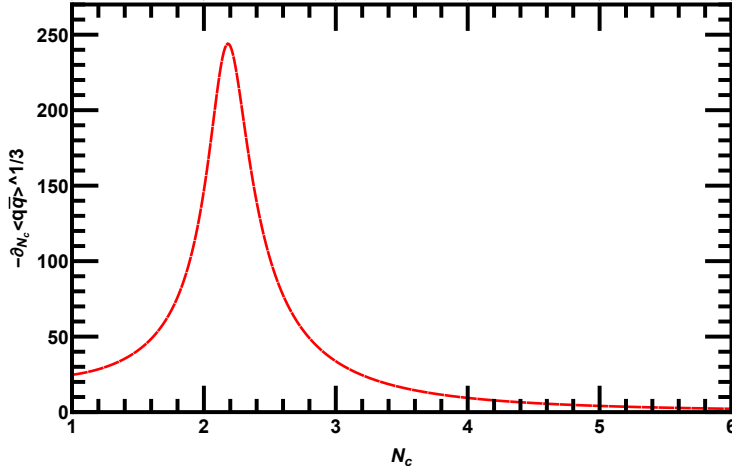


Figure 3. Color-gradient of quark-antiquark condensate for various N_c , for $N_f = 2$. The critical number of colors $N_c^c \approx 2.2$ for chiral symmetry breaking.

inflection point of the flavor-gradient of the quark-antiquark condensate $-\partial_{N_f}\langle\bar{q}q\rangle^{1/3}$. Our results in this scenario agree with that obtained in Ref. [22]. In Fig. 7, we show the variation of critical number of flavors N_f^c versus critical number of colors N_c^c . The Fig. 7, clearly demonstrate that the critical value N_f^c enhances with as the N_c^c shifted toward its larger values, and thus both the parameters opposes the effect of each other. For lower N_c^c , the N_f^c has a smaller values while for higher values of N_c^c , the N_f^c enhances. As, we discussed before that the number colors N_c anti-screens the strong interactions while N_f^c screens them and is readily confirmed from the Fig. 7. For clear understanding, we have tabulated some data for the variation of critical number of flavors N_f^c with various critical number of colors N_c^c in the Tab. 1.

In the next section, we shall discuss the dynamical chiral symmetry breaking and

Table 1. The variation of critical Number of flavors N_f^c with the critical number of colors N_c^c .

N_c^c	2.2	3	4	5	6	7	8	9	10
Critical N_f^c	3	8	9.5	10.3	10.7	11	11.2	11.3	11.4

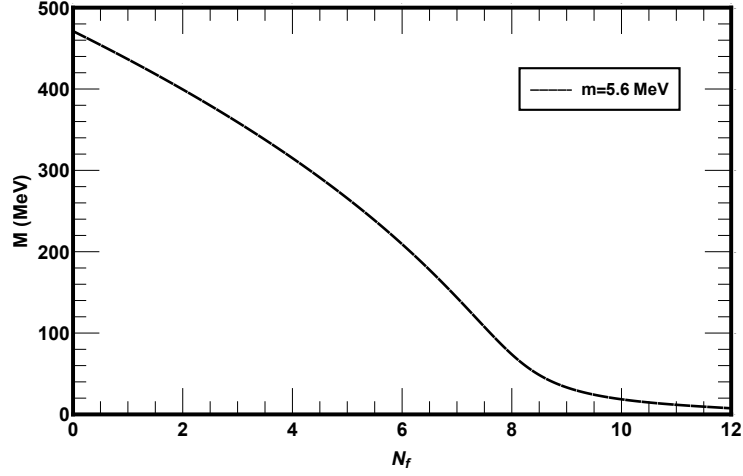


Figure 4. Behavior of the dynamical mass as a function of various number of flavor N_f with fixed number of colors $N_c = 3$. The dynamical mass monotonically decreases with increasing N_f .

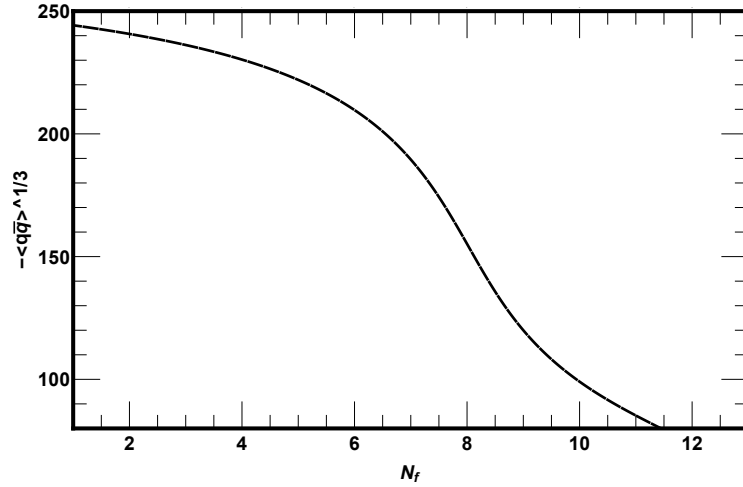


Figure 5. Quark-antiquark condensate as a function of number of flavors N_f with fixed colors $N_c = 3$.

its restoration with colors N_c and flavors N_f and at finite temperature T .

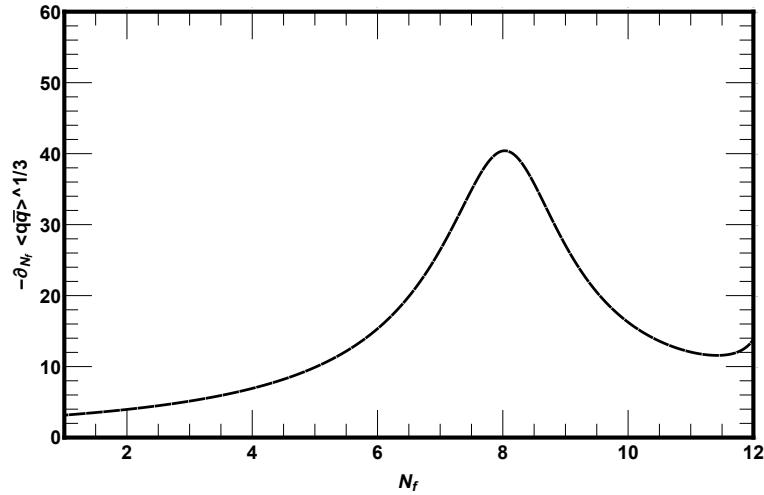


Figure 6. Flavor-gradient of the quark-antiquark condensate as a function of flavors N_f . The inflection point of the gradient represent the critical number of flavors for the dynamical chiral symmetry restoration and is at $N_f^c \approx 8$.

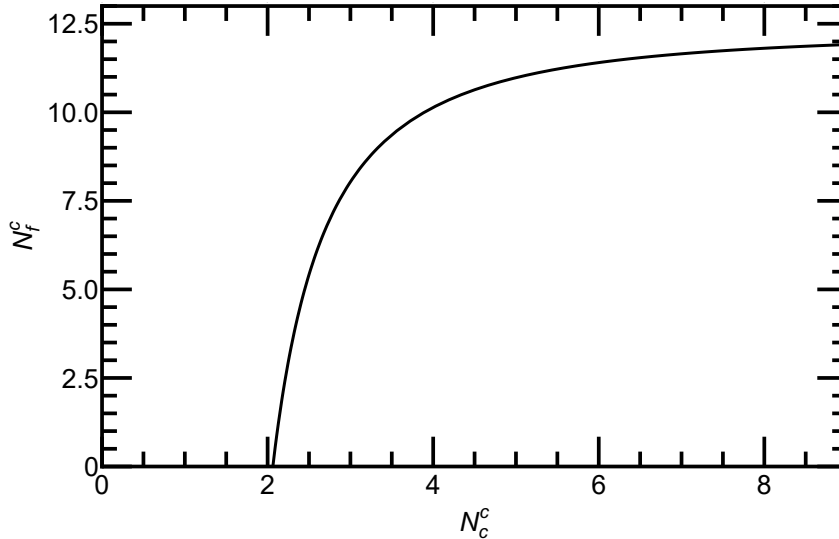


Figure 7. Behavior of the critical number of flavors N_f^c versus critical number of colors N_c^c for chiral symmetry breaking/restoration.

4. Dynamical chiral symmetry breaking with N_c , N_f and at finite T

In this section, we numerically solve the gap equation Eq. (22) to understand the dynamical symmetry breaking and restoration for colors N_c , and flavors N_f and at finite temperature T . Initially, we set $N_f = 2$ and plotted the dynamical mass in Fig. 8 as a function N_c , for various T and the corresponding condensate depicted in Fig. 9. We see that, upon increasing T , the dynamical symmetry is broken above the critical value of colors N_c^c . We determine the N_c^c , for various values of T from the inflection points of

the color-gradient $-\partial_{N_c} \langle \bar{q}q \rangle^{1/3}$, as shown in the Fig. 10. The peaks of the gradients shifts toward larger values of N_c^c as we increase T . This is because, on one hand N_c strengthens the interactions while T suppresses them and as a result, we needed large number of critical colors N_c^c for the dynamical chiral symmetry breaking. Next, we set $N_c = 3$,

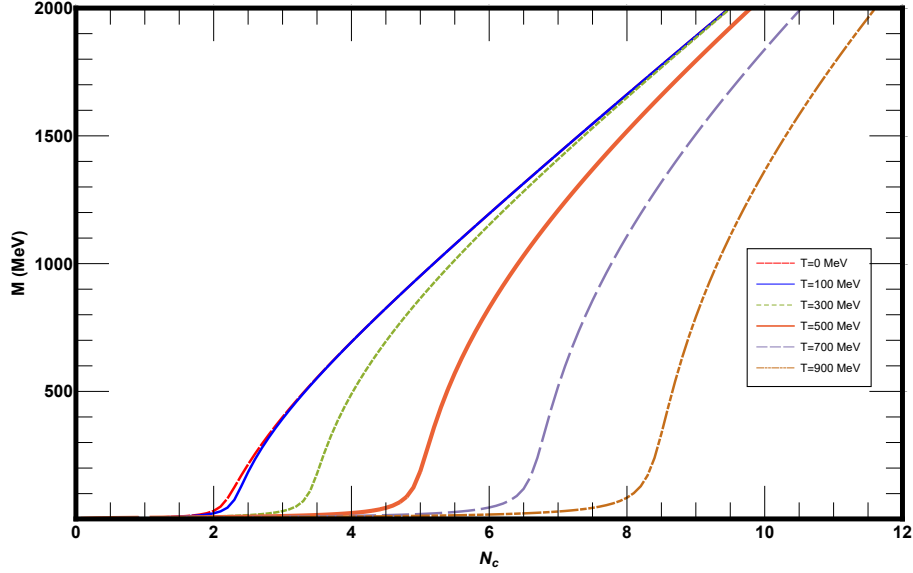


Figure 8. Behavior of dynamical mass as a function of N_c for two flavors $N_f = 2$, and for various temperatures T . The higher the temperature T the large number of critical number of colors N_c^c required for the dynamical symmetry breaking.

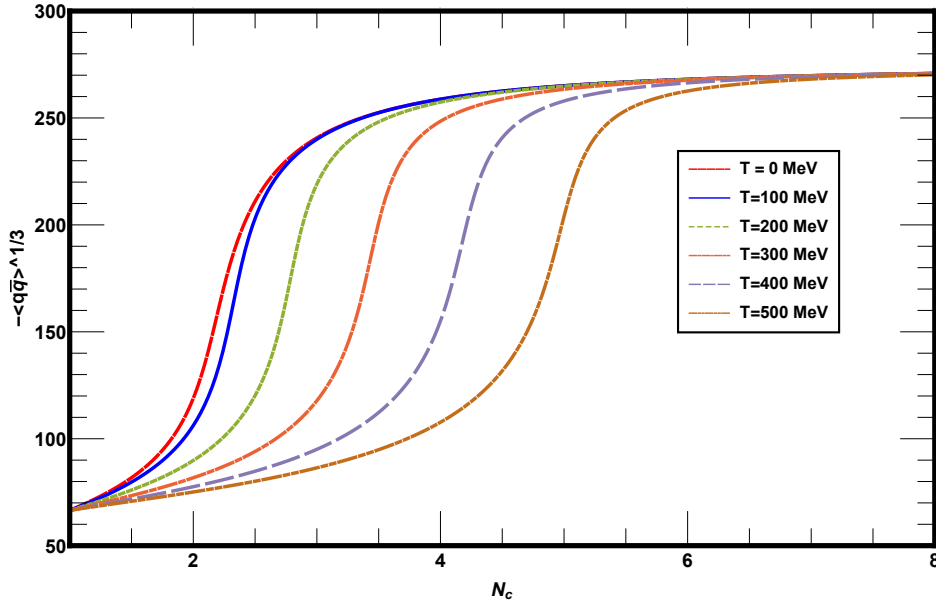


Figure 9. Quark-antiquark condensate as a function of N_c , for various T and for two flavors $N_f = 2$.

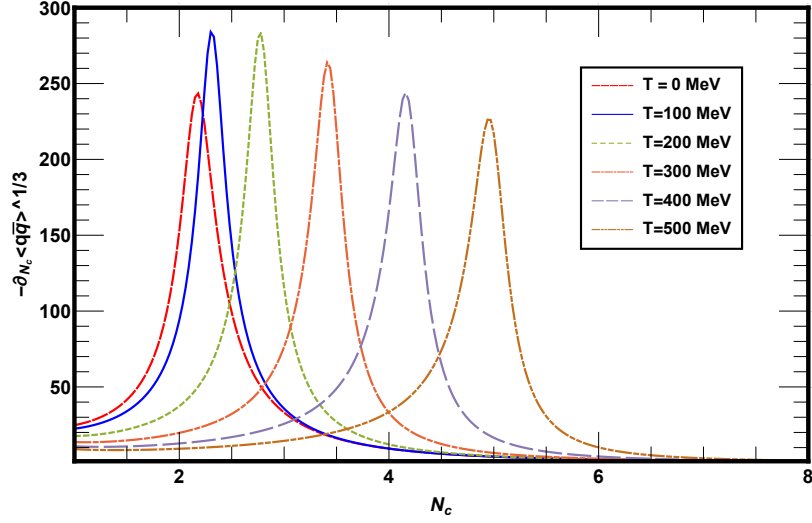


Figure 10. The color-gradient of quark-antiquark condensate for various temperatures T . The inflection points of the gradient shifted toward their larger values of critical number of colors N_c^c upon increasing the temperature T .

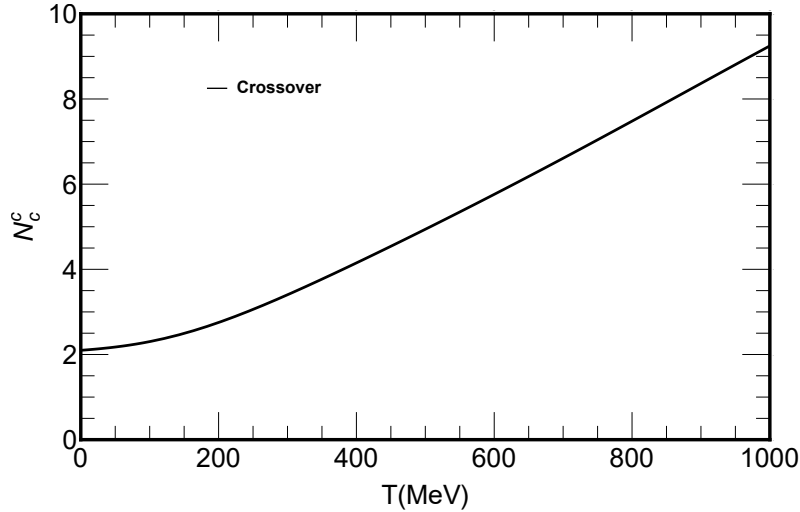


Figure 11. The phase diagram for the dynamical chiral symmetry breaking/restoration for critical number of colors N_c^c versus critical temperature $T = T_c$.

and plotted the dynamical mass as a function of N_f , for different values of T in Fig. 12 and the corresponding quark-antiquark condensate in the Fig. 13. In this case, we found that the dynamical mass as a function N_f suppresses as the T increases. This is because both the parameters, N_f and T screens the strong interactions, and thus, the dynamical chiral symmetry breaks even for smaller values of N_f . We thus, obtained the critical number of flavors N_f^c , for different T from the inflection points of the flavor-gradient $-\partial_{N_f} \langle \bar{q}q \rangle^{1/3}$, as depicted in the Fig. 14. We noted that the peaks are shifted toward their lower N_f^c values. We thus, observe that N_f^c monotonically decreases as T increases,

as demonstrated in the Fig. 15. This means that in the presence of heat both, less number of critical flavors N_f^c required for the chiral symmetry breaking and restoration. The nature of the transition at each temperature $T = T_c$ is observed to be cross-over.

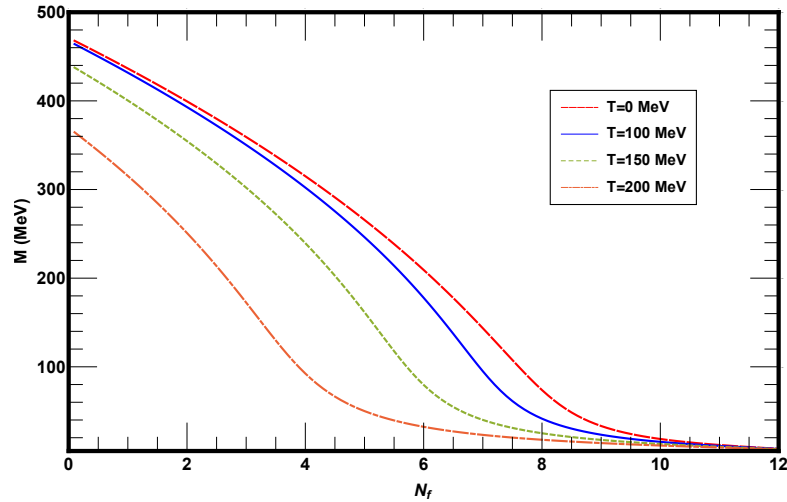


Figure 12. The behavior of dynamical mass as a function of number of flavors N_f , for fixed $N_c = 3$ and for various temperature T . Upon increasing the temperature T the dynamical mass suppresses.

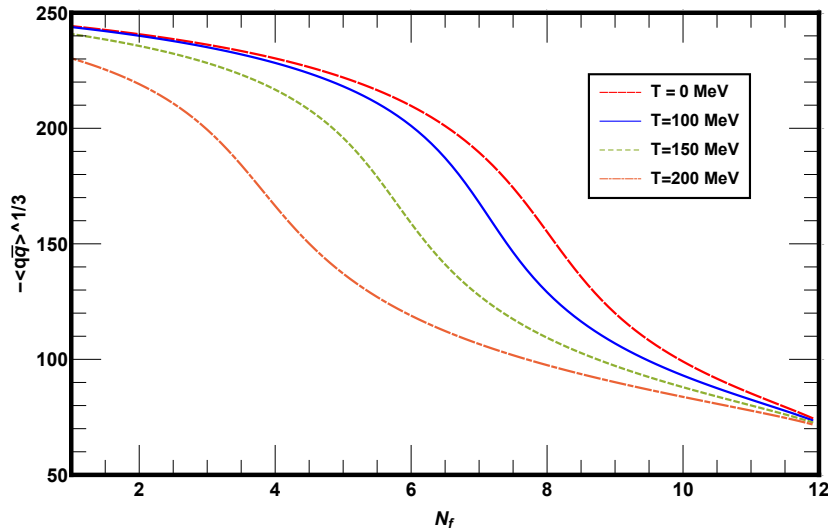


Figure 13. The behavior of quark-antiquark condensate as a function of number of flavors N_f , for fixed $N_c = 3$ and for various temperature T .

In the next section, we shall investigate the behavior of chiral symmetry breaking and restoration at a finite chemical potential μ upon increasing both the number of colors N_c and flavors N_f .

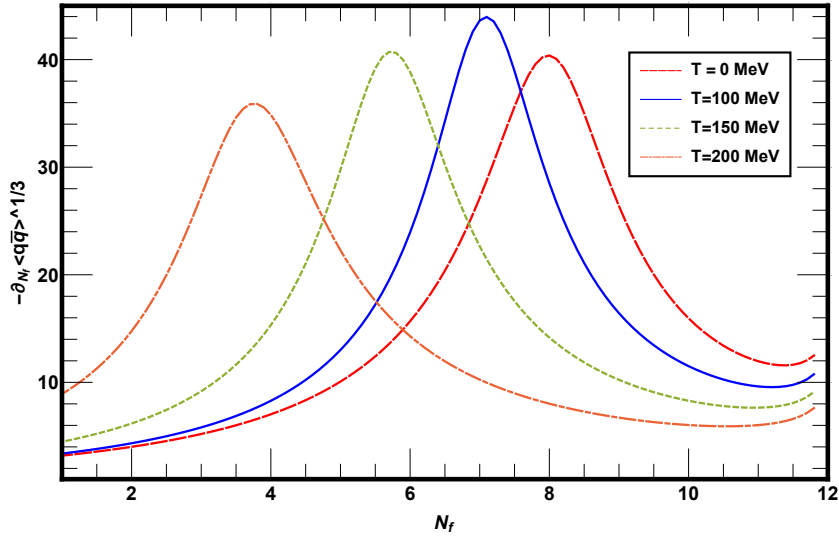


Figure 14. The flavor-gradient of the condensate at different temperature T , which shows that upon increasing the temperature the inflection points shifts toward their lower N_f^c values.

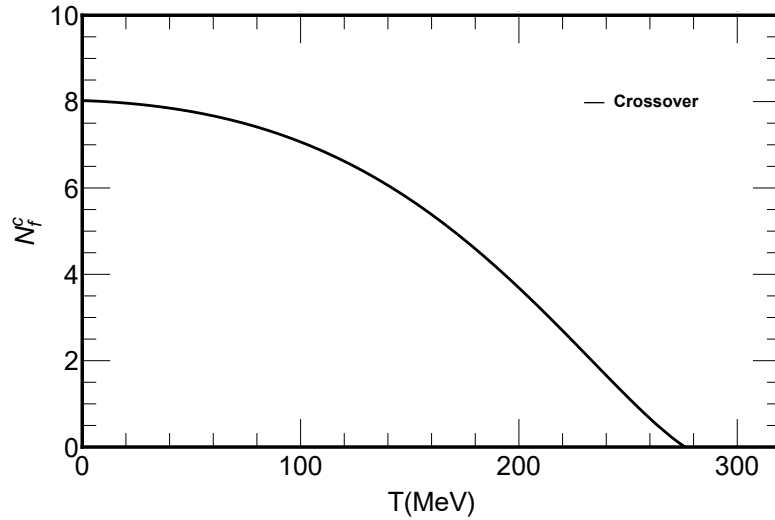


Figure 15. The phase diagram for the dynamical chiral symmetry breaking/restoration for critical number of flavors N_f^c versus critical temperature $T = T_c$.

5. Dynamical Chiral Symmetry Breaking for N_f , N_c and at finite μ

In the present section, we discuss the dynamical chiral symmetry breaking and its restoration at finite quark chemical potential μ , for various N_c and N_f . The dynamical mass as a function of μ for various N_c is shown in Fig. 16. We see that the dynamical chiral symmetry is partially restored when the chemical potential μ exceeds a critical value μ_c . The discontinuity in the dynamical mass around μ_c^c shows that the nature of the phase transition is of first-order, while the smooth decrease in the dynamical mass,

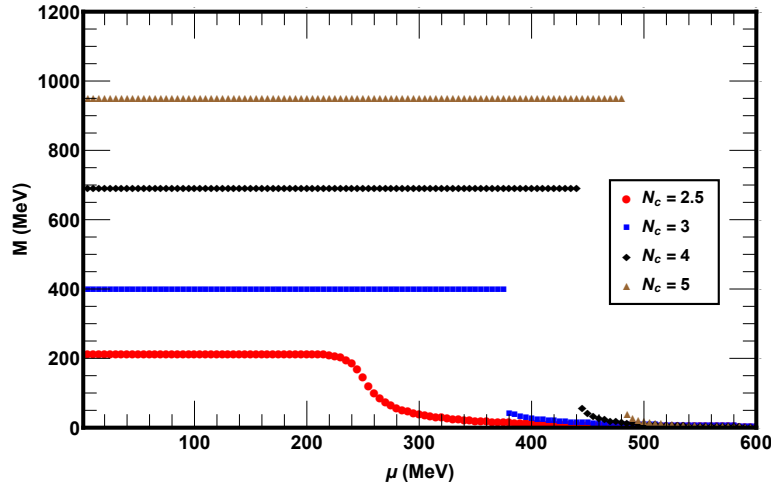


Figure 16. Behavior of the dynamical quark mass as a function of quark chemical potential μ for various number of colors N_c . The Plot show that the dynamical chiral symmetry restored above some critical μ_c , for each N_c .

represents the cross-over phase transition. It means that quark chemical potential μ , produces the screening effect, in contrast to the anti-screening produced by higher N_c . We determined the critical number of colors N_c^c from the inflection point of the color-gradient $-\partial_{N_c} \langle \bar{q}q \rangle_\mu^{1/3}$ at different μ , and plotted the variation of the N_c^c versus μ in the Fig. 17. This plot show that with an increase in chemical potential μ , the critical

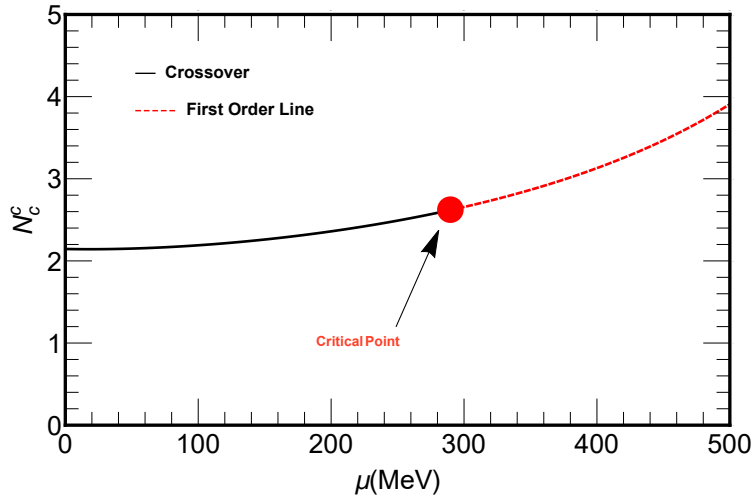


Figure 17. The phase diagram for the dynamical chiral symmetry breaking/restoration for critical number of colors N_c^c versus critical chemical potential $\mu = \mu_c$. The nature of the phase transition is smooth cross-over until the critical endpoint ($N_c^c \approx 2.5, \mu_c^c \approx 290$ MeV), and above this point the transition changes to the first order.

number of colors N_c^c for chiral symmetry breaking also increases. For example, at $\mu = 100$ MeV, the chiral symmetry breaking needs less critical number of colors (i.e,

$N_c^c = 2.2$) as compared to $\mu = 250$ MeV (i.e., $N_c^c = 2.5$). We found the cross-over phase transition for $N_c \leq 2.5$, and first order for $N_c > 2.5$ differentiated by a critical endpoint ($N_c^c \approx 2.5$, $\mu_c^c \approx 290$ MeV). In Fig. 18, we plotted the dynamical generated mass as a function of μ , for various number of flavors N_f and for fixed $N_c = 3$. The dynamical chiral symmetry is partially restored when the chemical potential reaches its critical value μ_c for various N_f . However, the nature of phase transition is off first-order for $N_f \leq 5$, and cross-over for $N_f \geq 5$. The dynamical mass as a function of chemical potential μ suppresses with the increase of N_f . Thus, the chemical potential μ also screens the interactions in resemblance with the screening effect produced by N_f . We determined the critical number of flavors N_f^c for each chemical potential μ from the

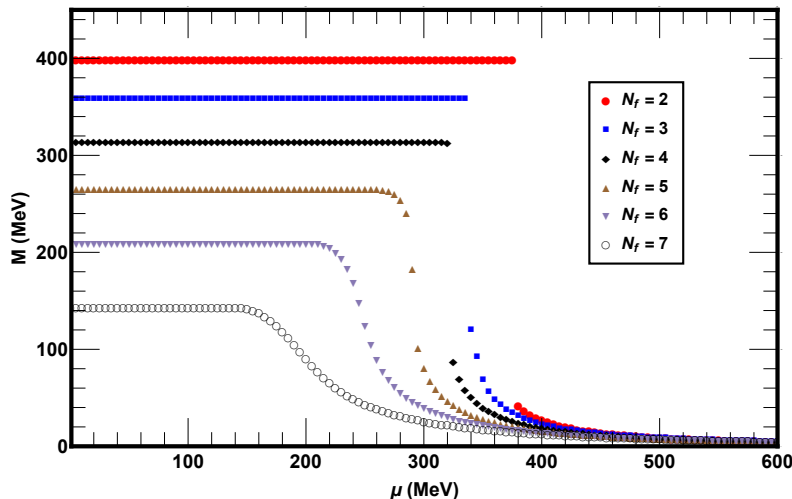


Figure 18. Behavior of the dynamical quark mass as a function of quark chemical potential μ for various number of flavors N_f . The plot show that the dynamical chiral symmetry restored above some critical μ_c , for each N_c .

inflation point of $-\partial_{N_c} \langle \bar{q}q \rangle_\mu^{1/3}$, and plotted the variation of the N_f^c versus critical chemical potential μ_c in the Fig. 19. We noted that the critical number of flavors N_f^c decreases with the increase of chemical potential μ . The nature of the phase transition is off first-order until the critical endpoint ($N_c^c = 5$, $\mu_c^c = 290$ MeV), where the transition changes to first order. The overall results show that at higher values of chemical potential μ , we need the higher critical number of colors N_c^c and the less critical number of flavors N_f^c required for the dynamical chiral symmetry breaking/restoration. In the next section, we investigate the simultaneous effects of temperature T and chemical potential μ on chiral phase transition with the higher number of light quark flavors and colors.

6. QCD Phase Diagrams for various N_c and N_f in $T - \mu$ plane

In this section, we sketched the QCD phase diagrams in the $T - \mu$ plane for various N_c and N_f . First, we sketch the QCD phase diagram in the Fig. 20, for fixed $N = 2$ and for various number of colors (i.e., $N_c = 3, 4, 5, 6$), at finite temperature T and chemical

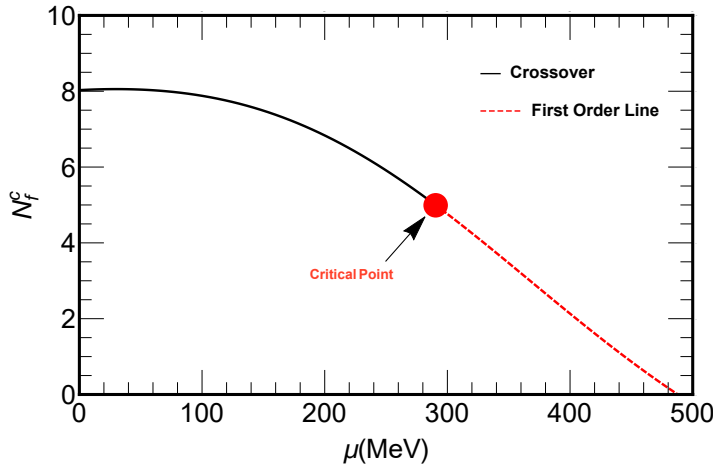


Figure 19. The phase diagram for the dynamical chiral symmetry breaking/restoration for critical number of flavors N_f^c versus critical chemical potential $\mu = \mu_c$. The nature of the phase transition is smooth cross-over for $N_f \geq 5$, while for $N_f \geq 5$ the transition changes to first order. Both transition are differentiated by a critical endpoint ($N_c^f \approx 5$, $\mu_c^f \approx 290$ MeV).

potential μ . We obtained the critical temperature T_c and critical chemical potential μ_c from the inflection points of the thermal and chemical potential gradients of quark-antiquark condensate, respectively. Initially, we plotted the phase diagram for $N_f = 2$ and $N_c = 3$, which show that at finite T but at $\mu = 0$, the dynamical chiral symmetry broken for temperature $T \leq T_c \approx 235$ MeV, while above, it is partially restored. The nature of the phase transition is cross-over in this case. At finite μ and at $T = 0$, the dynamical symmetry is observed to be broken below $\mu_c \approx 380$ MeV, while above, it is restored via first-order phase transition. It is confirmed from the Fig. 20 that the cross-over line in the phase diagram started from finite T -axis (for $\mu = 0$) never ends up at finite μ -axis (for $T = 0$) and hence, there is a critical endpoint where the cross-over transition changes to first order. We determined the co-ordinates of the critical endpoint at $(\mu_c^E \approx 330, T_c^E \approx 81)$ MeV. Our observation for $N_f = 2$ and $N_c = 3$ with a particular choice of NJL model parameters, is consistent with the QCD phase diagram sketched in [41]. Then, we extended it to various higher number of colors N_c . The solid-triangular line represents the cross-over phase transition for various N_c phase diagrams and the dotted dashed line for first order phase transition separated by the big red dots (the critical endpoints) in all the phase diagrams. We observed that the T_c , μ_c and co-ordinates of the critical endpoints (μ_c^E, T_c^E) are shifted toward their higher values upon increasing N_c . This is because, the N_c anti-screens the interaction, while T and μ produced the screening effect. The variation of the critical temperature T_c , the critical chemical potential μ_c , and the co-ordinates of critical endpoints (μ_c^E, T_c^E) with the number of colors N_c are tabulated in the Tab. 2. Next, we draw the QCD phase diagrams in the Fig. 21, for fixed $N_c = 3$, but for various number of light quark flavors (i.e., $N_f = 2, 3, 4, 5$). We used the same technique and same parameters for drawing the

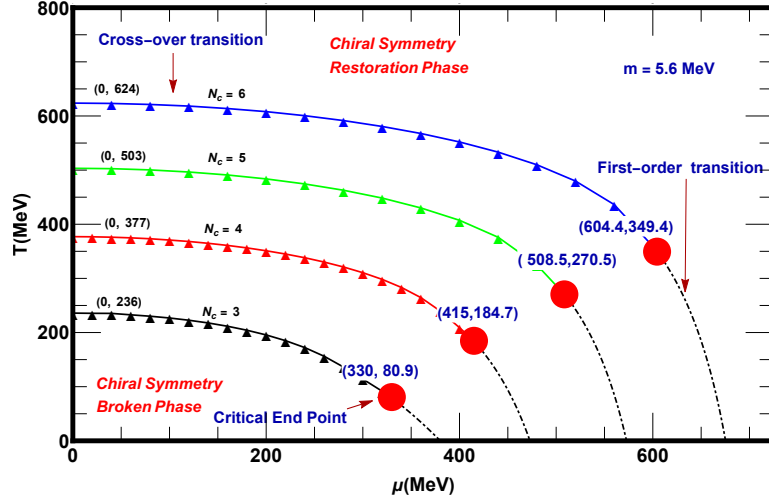


Figure 20. QCD phase diagram for T_c versus μ_c , for various number of colors ($N_c = 3, 4, 5, 6$) with fixed $N_f = 2$. All solid-triangle line represent the cross-over phase transitions and dot-dashed lines for first order phase transition. The big red-dots for the critical endpoint in each phase diagrams.

Table 2. Data for the variation of the critical temperatures T_c , the critical end point (μ_c^E, T_c^E) in the phase diagrams with various number of colors N_c and for fixed $N_f = 2$.

S.No	N_c	$m(\text{MeV})$	$T_c(\text{in MeV})$ at $\mu = 0$	$(\mu_c^E, T_c^E)(\text{MeV})$
01	3	5.6	235	(330, 81)
02	4	5.6	377	(415, 185)
03	5	5.6	503	(509, 271)
04	6	5.6	623	(604, 349)

phase diagram, but now we fixed $N_c = 3$ and for various number of light quark flavors N_f . All the phase diagrams in Fig. 21, shows their regular behaviors but suppresses with increasing number of flavors N_f . We noticed that, upon varying flavors N_f , the critical temperature T_c , the critical chemical μ_c potential and the coordinates of the critical endpoints (μ_c^E, T_c^E) decreases with the increase of N_f . This is because, all the three parameters N_f , T and μ screens the interactions. We show the variation of the critical temperature T_c , the critical chemical potential μ_c , and co-ordinates of critical endpoint (μ_c^E, T_c^E) with the number of flavors N_f in the the Tab. 3.

In the next section, we summarize our findings and draw the conclusions.

7. Summery and Conclusions

In this work, we have studied the dynamical chiral symmetry breaking/restoration for light quark flavors N_f and colors N_c . Also, we investigated the impact of N_c and N_f on

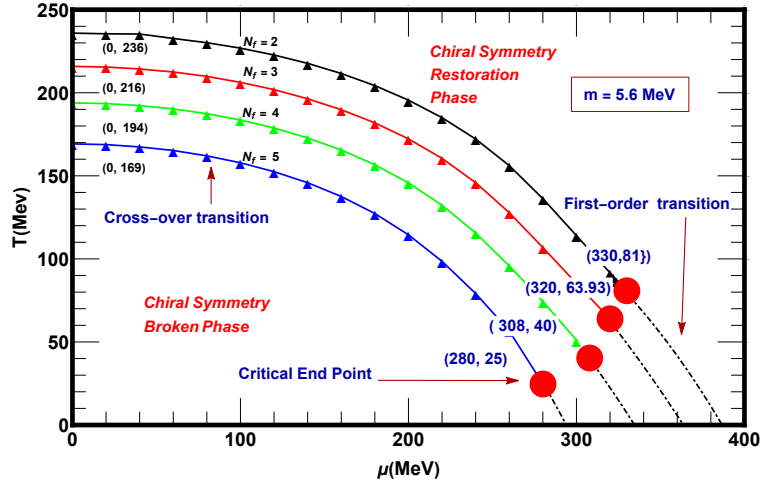


Figure 21. QCD phase diagram for T_c versus μ_c , for various number of flavors ($N_c = 2, 3, 4, 5$) with fixed number of colors $N_c = 3$. All solid-triangle lines represent the cross-over phase transitions and dot-dashed lines for first order phase transition. The big red-dots for the critical endpoint in each phase diagram.

Table 3. Data for the variation of the critical temperatures T_c , the critical end points (μ_c^E, T_c^E) in the phase diagrams with various number of flavors $N_f = 2$ and for fixed $N_c = 3$.

S.No	N_f	$m(\text{MeV})$	T_c (MeV) at $\mu = 0$	CEP(μ_c^E, T_c^E) (MeV)
01	2	5.6	235	(330, 81)
02	3	5.6	216	(320, 64)
03	4	5.6	194	(308, 40)
04	5	5.6	169	(280, 25)

the QCD phase diagram at finite temperature T and quark chemical potential μ . For this purpose, we used the NJL model dressed with the color-flavor dependence of effective coupling $\mathcal{G}^{N_c}(N_f)$, which has advantages to study the QCD gap equation not only for $N_f = 0$ but also for the higher number of flavors N_f . Our observations show that for fixed $N_c = 3$ and upon increasing N_f , the dynamical chiral symmetry is partially restored when N_f exceeds a critical value $N_f^c \approx 8$. Our results have a remarkable resemblance with the modern Lattice QCD simulation and Schwinger-Dyson's equations predictions. For $N_f = 2$, upon increasing the colors N_c , we determined the critical number of colors $N_c^c \approx 2.2$, above which the dynamical chiral symmetry is broken. The dramatic opposed effects between the two parameters N_f^c and N_c^c has been observed. This is by our expectation and conformation of the previous studies [22], that is, increasing number of flavors N_f screens the interactions while an increasing number of colors N_c anti-screens them.

At finite temperature T , our results show that the dynamical chiral symmetry is partially

restored when T reaches its critical value T_c . The temperature T itself produces the screening effect in contrast to the anti-screening effect of colors N_c , consequently, the larger number of colors N_c is required for the chiral symmetry breaking. Thus, the critical value N_c^c (for $N_f = 2$) enhances as T increases. For $N_c = 3$, and upon increasing N_f , we find that both T and N_f , screens the interactions and hence, less number of critical flavors N_f^c needed to restored the dynamical chiral symmetry. As a result, the N_f^c suppresses as T increases. The nature of the phase transition remains cross-over throughout for both (N_c^c versus T_c) and (N_f^c versus T_c) phase diagrams, respectively. Similarly, in the presence of quark chemical potential μ , we concluded that the critical value of color N_c^c for the dynamical chiral symmetry restoration, enhances as μ increases and vice verse. This is because the chemical potential μ itself screens the strong interaction. The nature of the phase transition, in this case, is observed to be smooth cross-over until the critical endpoint ($N_c^{cp} \approx 2.5, \mu_c^{cp} \approx 290$ MeV) while above, the transition changes to the first order. We further noticed that the critical number of light quark flavors N_f^c , required for the dynamical symmetry restoration suppressed with the increase of μ , because both N_f and μ produced the screening effect. In this case, the nature of the phase transition is smooth cross-over until the critical endpoint ($N_f^{cp} \approx 5, \mu_f^{cp} \approx 290$ MeV) while above, the transition changes to the first-order. Finally, we sketched the QCD phase diagram at finite temperature $T - \mu$ plane, for various N_c and N_f . We find that the critical temperature T_c , the critical chemical potential μ_c and the location of critical endpoint (μ_c^E, T_c^E) shifted toward higher values, with the increasing number of colors N_c . While in case of increasing flavors N_f , the situation is opposite i.e., the critical temperature T_c , the critical chemical potential μ_c and the critical endpoint (μ_c^E, T_c^E) shifted towards their lower values with the increasing number of flavors N_f . We conclude that considering the number of light quark flavors (or colors) yields an important impact on the QCD phase diagram, besides the heat bath and background fields. This work not only connects the color-flavor dependence with temperature T and chemical potential μ in congruence with the existing theoretical and phenomenological interpretation but also has important consequences related to the heavy-ion collision experiments. Soon, we plan to investigate the color-flavor phase diagram in the presence of background fields and other light hadrons properties.

Acknowledgments

We thanks to A. Bashir and A. Raya for their valuable suggestions and guidance during the completion of this manuscript. We acknowledge the organizers and participants of the “19th International Conference on Hadron Spectroscopy and Structure in memoriam Simon Eidelman (HADRON-2021), Mexico (online)” and “International Union of on Pure and Applied Physics (IUPAP-2022) Pakistan (Online)”, for providing a nice environment for exchange of ideas during presentation of this work, which led to the genesis of this manuscript. We also thanks to the colleagues of Institute of Physics, Gomal University for their encouragement.

References

- [1] Gross D J and Wilczek F 1973 *Phys. Rev. Lett.* **30** 1343–1346
- [2] Politzer H D 1973 *Phys. Rev. Lett.* **30** 1346–1349
- [3] Wilson K G 1974 *Phys. Rev. D* **10** 2445–2459
- [4] Appelquist T, Fleming G T and Neil E T 2009 *Phys. Rev. D* **79** 076010 (*Preprint* 0901.3766)
- [5] Bashir A, Raya A and Rodriguez-Quintero J 2013 *Physical Review D* **88** 054003
- [6] Appelquist T *et al.* (LSD) 2014 *Phys. Rev. D* **90** 114502 (*Preprint* 1405.4752)
- [7] Caswell W E 1974 *Phys. Rev. Lett.* **33** 244
- [8] Banks T and Zaks A 1982 *Nucl. Phys. B* **196** 189–204
- [9] Gies H and Jaeckel J 2006 *The European Physical Journal C-Particles and Fields* **46** 433–438
- [10] Appelquist T, Fleming G T and Neil E T 2008 *Phys. Rev. Lett.* **100** 171607 [Erratum: *Phys.Rev.Lett.* 102, 149902 (2009)] (*Preprint* 0712.0609)
- [11] Hasenfratz A 2010 *Physical Review D* **82** 014506
- [12] Aoki Y, Aoyama T, Kurachi M, Maskawa T, Nagai K i, Ohki H, Shibata A, Yamawaki K and Yamazaki T 2012 *arXiv preprint arXiv:1202.4712*
- [13] Appelquist T *et al.* (LSD) 2010 *Phys. Rev. Lett.* **104** 071601 (*Preprint* 0910.2224)
- [14] Hayakawa M, Ishikawa K I, Osaki Y, Takeda S, Uno S and Yamada N 2011 *Phys. Rev. D* **83** 074509 (*Preprint* 1011.2577)
- [15] Cheng A, Hasenfratz A, Petropoulos G and Schaich D 2013 *JHEP* **07** 061 (*Preprint* 1301.1355)
- [16] Hasenfratz A and Schaich D 2018 *JHEP* **02** 132 (*Preprint* 1610.10004)
- [17] Appelquist T *et al.* (Lattice Strong Dynamics) 2019 *Phys. Rev. D* **99** 014509 (*Preprint* 1807.08411)
- [18] Appelquist T, Cohen A G and Schmaltz M 1999 *Phys. Rev. D* **60** 045003 (*Preprint* hep-th/9901109)
- [19] Hopfer M, Fischer C S and Alkofer R 2014 *JHEP* **11** 035 (*Preprint* 1405.7031)
- [20] Doff A and Natale A A 2016 *Phys. Rev. D* **94** 076005 (*Preprint* 1610.02564)
- [21] Binosi D, Roberts C D and Rodriguez-Quintero J 2017 *Phys. Rev. D* **95** 114009 (*Preprint* 1611.03523)
- [22] Ahmad A, Bashir A, Bedolla M A and Cobos-Martínez J J 2021 *J. Phys. G* **48** 075002 (*Preprint* 2008.03847)
- [23] Bernard C, Burch T, Gregory E B, Toussaint D, DeTar C E, Osborn J, Gottlieb S, Heller U M and Sugar R (MILC) 2005 *Phys. Rev. D* **71** 034504 (*Preprint* hep-lat/0405029)
- [24] Cheng M *et al.* 2006 *Phys. Rev. D* **74** 054507 (*Preprint* hep-lat/0608013)
- [25] Bazavov A *et al.* 2012 *Phys. Rev. D* **85** 054503 (*Preprint* 1111.1710)
- [26] Bhattacharya T *et al.* 2014 *Phys. Rev. Lett.* **113** 082001 (*Preprint* 1402.5175)
- [27] de Forcrand P, Langelage J, Philipsen O and Unger W 2014 *Phys. Rev. Lett.* **113** 152002 (*Preprint* 1406.4397)
- [28] Bazavov A, Ding H T, Hegde P, Karsch F, Laermann E, Mukherjee S, Petreczky P and Schmidt C 2017 *Phys. Rev. D* **95** 074505 (*Preprint* 1701.03548)
- [29] Guenther J N 2021 *Eur. Phys. J. A* **57** 136 (*Preprint* 2010.15503)
- [30] Qin S x, Chang L, Chen H, Liu Y x and Roberts C D 2011 *Phys. Rev. Lett.* **106** 172301 (*Preprint* 1011.2876)
- [31] Fischer C S, Luecker J and Mueller J A 2011 *Phys. Lett. B* **702** 438–441 (*Preprint* 1104.1564)
- [32] Ayala A, Bashir A, Dominguez C A, Gutierrez E, Loewe M and Raya A 2011 *Phys. Rev. D* **84** 056004 (*Preprint* 1106.5155)
- [33] Gutiérrez E, Ahmad A, Ayala A, Bashir A and Raya A 2014 *Journal of Physics G: Nuclear and Particle Physics* **41** 075002
- [34] Eichmann G, Fischer C S and Welzbacher C A 2016 *Phys. Rev. D* **93** 034013 (*Preprint* 1509.02082)
- [35] Gao F and Liu Y x 2016 *Phys. Rev. D* **94** 076009 (*Preprint* 1607.01675)

- [36] Ahmad A and Raya A 2016 *Journal of Physics G: Nuclear and Particle Physics* **43** 065002
- [37] Fischer C S 2019 *Prog. Part. Nucl. Phys.* **105** 1–60 (*Preprint* 1810.12938)
- [38] Shi C, He X T, Jia W B, Wang Q W, Xu S S and Zong H S 2020 *JHEP* **06** 122 (*Preprint* 2004.09918)
- [39] Ahmad A 2021 *Chin. Phys. C* **45** 073109 (*Preprint* 2009.09482)
- [40] Klevansky S 1992 *Reviews of Modern Physics* **64** 649
- [41] Buballa M 2005 *Physics Reports* **407** 205–376
- [42] Costa P, Ruivo M C, De Sousa C A and Hansen H 2010 *Symmetry* **2** 1338–1374
- [43] Marquez F, Ahmad A, Buballa M and Raya A 2015 *Physics Letters B* **747** 529–535
- [44] Ahmad A, Ayala A, Bashir A, Gutiérrez E and Raya A 2015 *J. Phys. Conf. Ser.* **651** 012018
- [45] Ayala A, Flores J A, Hernandez L A and Hernandez-Ortiz S 2018 *EPJ Web Conf.* **172** 02003 (*Preprint* 1712.00187)
- [46] Ayala A, Hernández L A, Loewe M and Villavicencio C 2021 *Eur. Phys. J. A* **57** 234 (*Preprint* 2104.05854)
- [47] Nambu Y and Jona-Lasinio G 1961 *Physical Review* **124** 246
- [48] Ahmad A, Martínez A and Raya A 2018 *Phys. Rev. D* **98** 054027 (*Preprint* 1809.05545)